Title: FGF-2 Stimulates the Growth of Tenogenic Progenitor Cells to Facilitate the Generation of *Tenomodulin*-positive Tenocytes in a Rat Rotator Cuff Healing Model

Running title: Effect of FGF-2 on Rotator Cuff Healing

Abstract

Background: Fibroblast growth factor (FGF)-2 has the potential to enhance tendon-to-bone healing after rotator cuff (RC) injury.

Hypothesis: FGF-2 stimulates tenogenic differentiation of progenitors to improve the biomechanical strength and histological appearance of repaired RCs in rats.

Study Design: Controlled laboratory study.

Methods: Adult male Sprague-Dawley rats (n = 156) underwent unilateral surgery to repair the supraspinatus tendon to insertion sites. The FGF-2-treated (gelatin hydrogel containing 5 μg of FGF-2) and control groups (gelatin hydrogel only) were compared to investigate the effects of FGF-2 at 2, 4, 6, 8, and 12 weeks postoperatively. Biomechanical testing was performed at 6 and 12 weeks. Semi-quantitative histological analysis and immunohistochemistry for the proliferating cell nuclear antigen (PCNA) was performed, and the expression of tendon-related markers, including *Scleraxis* (*Scx*) and *Tenomodulin* (*Tnmd*) were monitored by real-time reverse transcription polymerase chain reaction (RT-PCR) and *in situ* hybridization. SRY-box containing gene 9 (Sox9) expression was monitored by RT-PCR and immunohistochemistry. At 2 and 4 weeks, immunohistochemistry for mesenchymal stem cell (MSC) markers were also performed.

Results: The FGF-2-treated group demonstrated a significant improvement in mechanical strength at 6 and 12 weeks and significantly higher histological scores than the control at ≥4 weeks. The average incidence of PCNA-positive cells was significantly higher at 2 and 4 weeks, and more cells

expressing MSC markers were detected at the insertion site in the FGF-2-treated group. The expression level of *Scx* increased significantly in the FGF-2-treated group from 4 to 8 weeks, while the *Tnmd* level increased significantly from 4 to 12 weeks postoperatively. The localization of *Tnmd* overlapped with the locations of reparative tissues accompanying collagen fibers with an aligned orientation. The *Sox9* expression was significantly upregulated at 4 weeks in the FGF-2-treated group.

Conclusion: FGF-2 promotes growth of the tenogenic progenitor cells, which participates in tendon-to-bone healing, resulting in the biomechanical and histological improvement of repaired RC.

Clinical Relevance: These findings provide clues on the clinical development of regenerative repair strategies for RC injury.

Key Terms: FGF-2, rotator cuff healing, *Scleraxis*, *Tenomodulin*, *Sox9*, cell proliferation, tenogenic progenitors

What is known about the subject:

Rotator cuff (RC) tears are a common cause of shoulder pain and dysfunction that often require surgical repair. A relatively high repair failure rate (21.7%, 187/861 patients) was reported in a recent meta-analysis of 14 studies after RC surgical repair.[14] Various efforts (e.g., the application of growth factors or transplantation of mesenchymal stem cells) have been made to promote a reparative response.[7,8,9,24,28] Administration of the fibroblast growth factor 2 (FGF-2) has the potential to enhance the reparative response during the RC healing process;[9] however, little is known about the biological mechanism of the repair-promoting effect (improvement of biomechanical strength or histological appearance) by FGF-2 during RC healing.

What this study adds to existing knowledge:

In a rat model, the administration of FGF-2 to the healing tendon-bone interface after surgical repair of an acute supraspinatus injury improved the mechanical strength and histological appearance between the tendon and bone at ≥4 weeks. Moreover, the proliferation of cells expressing markers of mesenchymal stem cells was stimulated in the FGF-2-treated group during the early phase of RC healing. Subsequently, upregulation of the tendon markers such as *Scleraxis* (*Scx*) and *Tenomodulin* (*Tnmd*) were detected in the FGF-2-treated group at ≥4 weeks. Interestingly, localization of *Tnmd* mRNA overlapped with the locations of reparative tissues accompanying collagen fibers with an aligned orientation during RC healing.

This suggests that FGF-2 promotes the growth of tenogenic progenitor cells to participate in tendon-to-bone healing, resulting in the histological and biomechanical improvement of RC healing.

Introduction

A rotator cuff (RC) injury is one of the most common causes of shoulder pain and dysfunction, often requiring surgical repair. Despite great improvement in surgical techniques for repairing RC tears, a recent meta-analysis of 14 studies reported on an imaging assessment of the structural integrity of RC repair, and it demonstrated a high rate of failed repair (21.7 %, 187/861 patients) at the latest follow-up.[14] Therefore, developing new strategies for enhancing tendon-to-bone healing is imperative.

Various growth factors are endogenously expressed during tendon-to-bone healing, suggesting that they play critical roles in the repair process,[27] and there is an interest regarding their use as therapeutic agents for enhancing RC repairs. Of those, fibroblast growth factor-2 (FGF-2) is a potent mitogen for a wide variety of cells, including mesenchymal stem cells (MSCs) and progenitor cells.[11, 19, 25] We previously demonstrated that the local administration of FGF-2 accelerates the initial tendon-to-bone healing as indicated by biomechanical tests and histological analyses after supraspinatus tendon repair in rats.[9] However, the biological mechanism of the reparative enhancement by FGF-2 during RC healing is unclear.

Recently, several genes have been identified as specific tendon markers. Scleraxis (Scx) is a basic helix-loop-helix transcription factor that is expressed in both tenogenic progenitors and tenocytes.[13, 15] Tenomodulin (Tnmd) is a type II transmembrane protein that is specifically expressed in the dense connective tissues such as tendons and ligaments.[17, 18] Tnmd is detected in mature tenocytes and is

positively regulated by Scx.[3, 18] Identification of these marker genes enables us to study the cellular and molecular events that occur during the establishment of the osteotendinous junction in detail. Recently, we reported that a subset of *Scx*-positive progenitors with an expression history of *SRY-box containing gene 9* (*Sox9*) contributes to the formation of enthesis during development.[20]

The purpose of this study was to investigate the effects of FGF-2 administration on cell proliferation and the expression of enthesis-related marker genes (i.e., *Scx*, *Sox9*, and *Tnmd*) during RC tendon-to-bone healing in rats. The effects on biomechanical strength and histological appearance during healing were also investigated. We hypothesized that FGF-2 stimulates the tenogenic differentiation of progenitors and improves the biomechanical strength and histological appearance of repaired RCs in rats.

Materials and Methods

Study Design

This study was approved by our institution's Animal Studies Committee and the Institutional Animal Care and Use Committee. We used a rat RC healing model, in which the supraspinatus tendon insertion site was transected and surgically repaired immediately, to investigate the effects of FGF-2 on tendon-to-bone healing. In this model, a normal tendon-to-bone insertion site is not regenerated even after 16 weeks postoperatively.[23]

We included 156 adult male Sprague-Dawley rats (19–21 weeks old; mean weight, 475 ± 37 g) that underwent unilateral surgery for supraspinatus tendon repair immediately after transaction, and they were randomly allocated to the control or FGF-2-treated groups (n = 78 per group). In the control, gelatin hydrogel sheets (MedGEL Co., Kyoto, Japan) with a phosphate-buffered saline (PBS) were applied between the supraspinatus tendon and bone. In the FGF-2-treated group, gelatin hydrogel sheets containing 5 μg of rhFGF-2 (Kaken Pharmaceutical Co., Tokyo, Japan) were applied. All rats were sacrificed at 2, 4, 6, 8, or 12 weeks postoperatively. At each time point, 6 specimens per group were used for histological evaluation (i.e., histology, immunohistochemistry, or *in situ* hybridization), and 6 per group were analyzed with real-time reverse transcription polymerase chain reaction (RT-PCR). At 6 and 12 weeks, 9 specimens per group were used for biomechanical testing.

Local Administration of FGF-2

We used a biodegradable gelatin hydrogel sheet[21] (MedGel PI5, MedGEL Co) as a carrier for the FGF-2. In our pilot study, three doses of FGF-2 (0.5, 5, and 50 μg/site) in gelatin hydrogel sheets were compared between the carrier-only and suture-only groups using the same method in the present study (n = 6 per group underwent histological and biomechanical testing). At 12 weeks postoperatively, a significant improvement in the ultimate load-to-failure was achieved in all FGF-2-treated groups (0.5-μg, 29.1 ± 10.1 N; 5-μg, 31.7 ± 8.5 N; and 50-μg, 25.9 ± 8.6 N) compared to the carrier-only (15.8 ± 4.5 N) and suture-only groups (12.4 ± 2.4 N). The histological scores in the FGF-2-treated groups (0.5-μg, 9.7 ± 1.0; 5-μg, 10.7 ± 0.5; and 50-μg, 10.3 ± 0.5) were higher than that in the suture-only (7.5 ± 0.5) and carrier-only groups (7.8 ± 0.8). Although there were no significant differences among the three FGF-2-treated groups, we used the 5-μg dose of FGF-2, because the 5-μg FGF-2-treated group showed the highest histological score and the ultimate load-to-failure.

Before administration, freeze-dried gelatin hydrogel sheets (1 mg) for each shoulder were soaked with 10 μL of a PBS or FGF-2 (500 μg/mL), and the sheets were incubated for 60 min at room temperature (RT).

Surgical Procedure

The rats underwent left shoulder surgery, as previously described.[6, 23] Briefly, after the administration of general anesthesia with an intraperitoneal injection of pentobarbital (25–30 mg/kg),

longitudinal antero-lateral skin and deltoid muscle incisions were made, and the supraspinatus tendon was exposure. The supraspinatus tendon was detached sharply at its insertion (3 mm in the anterior-to-posterior dimension), and the fibrocartilaginous stump on the greater tuberosity was completely removed using a high-speed bur until bleeding was observed. A 0.8-mm drill hole was created transversely in an anterior-posterior orientation through the proximal part of the humerus. We sutured the torn supraspinatus tendon to its anatomic position using a double-armed 5-0 prolene suture (Ethicon, Somerville, NJ) using a modified Mason-Allen method. A gelatin hydrogel sheet soaked with PBS or FGF-2 was fixed to the torn end of the tendon using a 5-0 prolene suture, which is used for repair, and it was secured between the tendon and bone. The incision was closed in layers with 4-0 nylon sutures. All rats were permitted cage activities without immobilization postoperatively.

Biomechanical Testing

As previously described,[9, 26] 9 animals per group were tested at 6 and 12 weeks postoperatively, and 9 intact shoulders were used as a normal control. All specimens were frozen at -80°C until testing. After thawing, the supraspinatus tendon repair to the humerus was dissected from the surrounding tissues with a custom-designed double scalpel blade to a 2-mm-width to standardize the tendon tested, and the supraspinatus muscle belly and any scar tissue was removed. Each specimen was preloaded to 0.1 N and loaded to failure with a conventional tensile tester (STA1225; Orientec,

Tokyo, Japan) at a rate of 10 mm/min, and the ultimate load-to-failure and the failure site were recorded. The linear region of the load-displacement curve was used to calculate the stiffness. The cross-sectional area of the repaired insertion site, including its width and thickness, was measured using a digital micro-caliper.[7] The ultimate load-to-failure was divided by the cross-sectional area of the repair site to determine the ultimate stress-to-failure.

Histological Evaluation

The tissues were fixed overnight in 4% paraformaldehyde at an abduction angle of 30° and were decalcified in Morse's solution (10% sodium citrate and 22.5% formic acid). After decalcification, the tissues were dehydrated and were embedded in paraffin. The sections were viewed under an Olympus BX-51 microscope (Olympus Optical, Tokyo, Japan), and digital images were taken using a DP70 camera (Olympus Optical). To evaluate healing at the tendon-to-bone site semi-quantitatively, we used a computerized image analysis (Image J, National Institutes of Health, Bethesda, MD) and a modified scoring system (Table 1) based on previously reported histological evaluations.[24, 26, 28] We scored the healing insertion site according to three histological parameters (i.e., cellularity, vascularity, and collagen fiber orientation). Three sequential sections were obtained from each animal for each staining, and the results were averaged.

To analyze cellularity, all cell nuclei in a randomly selected region of interest (200 × 200 μm) were counted to calculate the number per mm^2 at the insertion site (100–400 μm proximal to the bone trough) on hematoxylin and eosin (HE)-stained slides under 100-fold magnification.

To analyze vascularity, all blood vessels were counted to calculate the mean vessel number from three sequential sections at the insertion site (100–400 μm proximal to the bone trough) on HE-stained slides under 100-fold magnification.

The collagen fiber orientation was assessed by picrosirius-red stained sections using a polarizing microscope.[7, 26] On eight-bit digitized images, intense white areas of brightly diffracted light on a gray scale (black, 0; white, 255), were observed. Higher gray scales indicated more organized collagen fibers. We randomly selected 10 square areas (100 × 100 μm) at the insertion site (100–400 μm proximal to the bone trough) under 12.5-fold magnification, and gray scales were measured using Image J. The values from the 10 areas were averaged to obtain a value of average gray scales per specimen. To reduce sampling errors, we took photomicrographs of three sequential sections from each specimen under the same illumination conditions.

Cellularity and collagen fiber orientation were scored using the percentage of the value measured in six right shoulders (intact side). A perfect score is 12 points (Table 1). Analysis was performed by two colleagues who were blinded to the groups for each specimen and the time points throughout the histological examinations.

Immunohistochemistry

Semi-serial sections (4 μm) were prepared for immunostaining. To assess the cell proliferation, the expression of Sox9 and existence of MSCs, we performed immunostaining for PCNA and Sox9 at all time points, MSC-related surface antigens (CD105, CD90, and CD73), and hematopoietic cell antigen (CD45 and CD34) at 2 and 4 weeks postoperatively.[2]

The sections were deparaffinized; rehydrated; and incubated overnight at 4°C with a primary antibody recognizing PCNA (dilution 1:200, clone PC10; Dakopatts, Copenhagen, Denmark), Sox9 (1:200, AB5535; Millipore, Billerica, MA), CD105 (1:50,#05-1424; Millipore), CD90 (1:200, AB225; Abcam, Cambridge, MA), CD73 (1:200, AB175396; Abcam), CD45 (1:1000, AB10558; Abcam), and CD34 (1:100, AB 64480; Abcam). Subsequent reactions were performed using a peroxidase-labeled antibody (Histofine Simple Stain Max PO; Nichirei, Tokyo, Japan), which reacted with a 3, 3-diaminobenzidine solution and were counterstained in 0.5% Mayer's hematoxylin.

Estimation of Cell Proliferation and the Expression of Sox9 at the Healing Site

To estimate cell proliferation at the healing site, we modified the previously described method for PCNA-positive cell counting.[12] Three square areas (200 × 200 μm) at the insertion site (100–400 μm proximal to the bone trough) were selected randomly under 200-fold magnification. The percentage

of PCNA-positive cells was calculated by dividing the number of PCNA-positive cells by the total number of cells in the area; the average percentage of three areas from each slide was recorded.

The percentage of Sox9-positive cells was calculated in the same manner.

RNA Isolation and Real-time Reverse Transcription Polymerase Chain Reaction Analysis

At all time points, the left (operative side) and right (intact side) tendon-to-bone tissues were dissected and flash frozen in liquid nitrogen and crushed using a Multi-beads Shocker (Yasui Kikai, Osaka, Japan). After homogenization, total RNA was extracted and purified per the manufacturer's instructions using the TRIzol Plus RNA Purification Kit (Invitrogen, Carlsbad, CA). The total RNA (1 μg) was reverse transcribed to complementary DNA (cDNA) using the Thermoscript RT kit (Invitrogen). Real-time PCR was performed using an ABI7500 system (Applied Biosystems, Foster, CA) with TaqMan Universal PCR Master Mix and TaqMan™ Gene Expression Assays for the following genes: *Scx* (Assay ID: Rn01504576_m1), *Tnmd* (Rn00574164_m1), *Sox9* (Rn01751069_mH), and *18S ribosomal RNA* (Rn03928990_g1). Each sample was analyzed in duplicate. The relative expression levels for the target genes were analyzed using the comparative Ct method. The delta-Ct values were calculated by the difference between the Ct values of the target genes and *18S ribosomal RNA*. The results are represented as the relative gene expression compared to the intact tendon.[16]

In situ Hybridization

In situ hybridization was performed to detect the expression of *Scx* and *Tnmd* mRNA as previously described.[1] Briefly, 5-μm sections were deparaffinized, rehydrated, incubated with proteinase K (20 μg/mL; Gibco BRL, Rockville, MO), post-fixed in 4% paraformaldehyde, acetylated with 0.1 M triethanolamine containing 0.25% acetic anhydride for 10 min, dehydrated, and air-dried.

Sense and antisense RNA probes labeled with digoxigenin (DIG) for *Scx* or *Tnmd* were synthesized by *in vitro* transcription with a DIG RNA labeling kit (Roche, Mannheim, Germany) using the following cDNA clones: rat *Scx* cDNA containing a 0.726 kb fragment was subcloned into pBSII SK+ (Stratagene, La Jolla, CA) and rat *Tnmd* cDNA containing a 0.607 kb fragment was subcloned into pCRII-TOPO (Invitrogen), as a template after linearization. Hybridization was performed at 50°C for 16 h. After hybridization, the sections were washed in 2 × SSC containing 50% formamide, treated with RNase A (20 μg/mL), and washed in 2 × SSC. Immunological probe detection was performed with an anti-DIG-AP Fab fragment (Roche) and BM Purple (Roche). The specificity of these antisense probes was confirmed on mouse embryo (E16.5) sections as positive controls. Sense probes for *Scx* and *Tnmd* were used on sections as negative controls.

Evaluation of the Association between the Locations of Reparative Tissue Accompanying Collagen Fibers with an Aligned Orientation and *Scx* or *Tnmd* mRNA

To investigate the correlation between the location of healing tissues with aligned collagen fiber orientation and the localization of *Scx* or *Tnmd* mRNA, images from picrosirius-red staining and *in situ* hybridization in sections in the treatment and control groups at 8 weeks postoperatively (n = 12) were evaluated, and nine areas (tendon, suture, and insertion areas of the articular side, middle, and bursal side) were set (see Figure 5C). Collagen fiber orientation for each area was evaluated by applying the gray scale as described above. Expression levels of *Scx* or *Tnmd* mRNA (density of hybridization signals) in each area were graded using previously reported[23] standards to define high (4), moderate (3), low (2), and undetectable (1) levels, and the highest grade for each area from each specimen was recorded.

Statistical Analysis

Before the study initiation, a power analysis was performed using the G*Power 3.1 program,[5] which we used in our pilot study described above that had a similar rat model. A minimum of 9 specimens per group for each time point was required for biomechanical testing (Cohen's d, ≥1.45), and a minimum of 6 specimens per group for each time point was required for histological evaluation (Cohen's d, ≥2.04), with an α value of 0.05 and a power of 0.80 based on the effect size. The sample size for real-time RT-PCR was determined according to the power analysis for histological evaluation. Our primary analysis compared measurements between the groups at each time point, and the secondary analysis compared measurements within the groups over time. We used

nonparametric statistical methods for all the analyses, because the data were non-normally distributed. Statistical significance between the groups at each time point was estimated using the Mann-Whitney U test. Differences in the measurements within groups over time were analyzed using the Kruskal-Wallis test, followed by the post-hoc Scheffe test for multiple comparisons. The correlation between the collagen fiber orientation and the expression levels of *Scx* or *Tnmd* mRNA were assessed using Spearman's correlation analysis. Values of $P < .05$ were considered statistically significant.

Results

Biomechanical Testing

Three of 9 specimens from the normal shoulders failed at the insertion site; the other 6 failed at the tendon mid-substance. All specimens from the operated groups failed at the site of surgical repair (Table 2).

At 6 weeks postoperatively, the ultimate load-to-failure, stiffness, and ultimate stress-to-failure were significantly higher in the FGF-2-treated group than in the control. No significant differences were observed between the groups in the cross-sectional area of the repair site.

At 12 weeks postoperatively, the ultimate load-to-failure and ultimate stress-to-failure were significantly higher in the FGF-2-treated group than in the control. No significant differences were observed between the groups in the stiffness and cross-sectional area of the repair site.

Histological Analysis

Effects of FGF-2 on the histological appearance

At 2 weeks postoperatively, hyper-cellular and hyper-vascular granulations were noted in the insertion site (Figure 1A, G), and areas of brightly diffracted polarized light were rarely observed at the insertion site in any of the groups (Figure 1D, J).

From 6 to 12 weeks, although granulations decreased compared to the previous time point, the tendon-to-bone area remained hyper-vascular and filled with disorganized collagen fibers in the

controls (Figure 1B, C, E, F). Conversely, in the FGF-2-treated groups, these granulations were decreased, and the area of brightly diffracted polarized light at the insertion site was larger than that in the controls (Figure 1H, I, K, L). The histological differences between the treatment and control group were observed at ≥4 weeks.

At the bone surface, normal fibrocartilaginous enthesis was not regenerated in any specimen from any group at any time point.

In both groups, cellularity and vascularity decreased, but the collagen fiber orientation and total histological scores increased with time (Table 3). The mean number of blood vessels at the insertion site was significantly smaller in the FGF-2-treated group than in the control at 8 and 12 weeks postoperatively. Collagen fiber orientation and the total score were significantly higher in the FGF-2-treated group than in the control at ≥4 weeks.

Effects of FGF-2 on cell proliferation

At 2 and 4 weeks postoperatively, greater numbers of PCNA-positive cells were observed in the granulation tissue between the tendon and bone in the FGF-2-treated group than those in the control (Figure 2A, C). At ≥6 weeks, PCNA-positive cells obviously decreased and were mainly present at the bone surface in both groups (Figure 2E). The percentage of PCNA-positive cells was significantly larger in the FGF-2-treated group than in the control at 2 weeks (45.4 ± 9.3% vs. 30.8 ± 5.7%; $P = .016$) and 4 weeks (41.9 ± 8.0% vs. 29.0 ± 7.4%; $P = .025$). There were no differences

between the groups at 6 weeks (control, 21.2 ± 4.6%; FGF-2-treated, 23.8 ± 5.3%; *P* = .423), 8 weeks (control, 19.7 ± 2.7%; FGF-2-treated, 22.3 ± 5.7%; *P* = .263) and 12 weeks (control, 19.0 ± 3.8%; FGF-2-treated, 19.6 ± 5.3%; *P* = .749) (Figure 2E).

Effect of FGF-2 on the expression of *Scx* and *Tnmd*

Real-time RT-PCR analysis showed that a significantly higher expression of *Scx* was detected in the FGF-2-treated group than in the control at 4, 6, and 8 weeks (*P* = .010, .010, and .004, respectively). There were no differences between the control and FGF-2 groups at 2 and 12 weeks (*P* = .631, and .150, respectively) (Figure 3A). *Tnmd* expression was significantly higher in the FGF-2-treated group than in the control at 4, 6, 8, and 12 weeks (*P* = .004, .010, .004, and .016, respectively). There were no differences between the groups at 2 weeks (*P* = .631) (Figure 3B). *Scx* expression was transiently upregulated from 4 to 8 weeks; meanwhile *Tnmd* expression was persistently upregulated by FGF-2 treatment even after 12 weeks postoperatively (Figure 3).

We then performed *in situ* hybridization to analyze the localization of *Scx* and *Tnmd* mRNA. In both groups, hybridization signals for *Scx* were detected in the spindle-shaped cells at the tendon mid-substance at all time points (Figure 4A, C, I, K), and a few hybridization signals for *Scx* were detected in the round and spindle-shaped cells within the granulation tissue around the suture at 4, 6, and 8 weeks (data not shown). In the control, hybridization signals for *Scx* were rarely detected within the fibro-vascular tissue at the bone surface at any time points (Figure 4E, G). However, in the

FGF-2-treated group, *Scx* were expressed in the spindle-shaped cells at the bone surface at ≥4 weeks (Figure 4M, O).

Tnmd signals were also detected in the spindle-shaped cells at the tendon mid-substance in both groups at all time points, and hybridization signals increased with time (Figure 4B, D, J, L). In the FGF-2-treated group, the distribution of these signals expanded into reparative tissues near the suturing site compared to the control. However, *Tnmd* was rarely detected at the bone surface in either group at any time point (Figure 4F, H, N, P).

Correlation between the locations of healing tissue with aligned collagen fiber orientation and *Scx* or *Tnmd* mRNA

We assessed 108 areas in both groups at 8 weeks postoperatively (Figure 5). A weak positive correlation between the location of aligned collagen fiber orientation and expression levels of *Scx* mRNA in each area was observed (Spearman's rank correlation [ρ] = .27, $P < .001$) (Figure 5D). Meanwhile, a strong positive correlation between the location of aligned collagen fiber orientation and the expression levels of *Tnmd* mRNA in each area was observed (ρ = .88, $P < .001$) (Figure 5E).

Effect of FGF-2 on Sox9 expression

Real-time RT-PCR analysis showed that *Sox9* expression was significantly higher in the FGF-2-treated group than in the control at 4 weeks ($P = .004$). However, at 2, 6, 8 and 12 weeks,

there were no statistically significant differences between the groups (P = .337, .749, .200 and, .337, respectively) (Figure 6).

In immunostaining for Sox9 (Figure 7), Sox9-positive cells were mainly observed at the tendon-to-bone insertion site, but a few Sox9-positive spindle-shaped cells were also detected at the tendon mid-substance at ≥ 4 weeks in both groups. The percentage of Sox9-positive cells was significantly higher in the FGF-2-treated group than in the control at 4 weeks (23.7 ± 4.9% vs. 14.0 ± 3.6%; P = .010). There were no differences between the groups at 2 weeks (control, 10.1 ± 4.8%; FGF-2-treated, 13.4 ± 6.6%; P = .337), 6 weeks (control, 19.7 ± 2.7%; FGF-2-treated, 22.3 ± 5.7%; P = .263), 8 weeks (control, 10.3 ± 1.1%; FGF-2-treated, 11.2 ± 1.5%; P = .423), and 12 weeks (control, 10.1 ± 2.6%; FGF-2-treated, 11.3 ± 3.4%; P = .749) (Figure 7I).

Effect of FGF-2 on mesenchymal stem cells marker-positive cells in the early phase of healing

To analyze MSCs, serial sections were immunostained for MSC-related surface antigens (CD105, CD90, and CD73) and hematopoietic cell antigen (CD45 and CD34) at 2 and 4 weeks postoperatively. CD45- and CD34-positive cells were rarely detectable at the insertion site in either group. In the FGF-2-treated group, cells positive for CD105, CD90, and CD73 were detected more within the reparative tissue at the insertion site than in the control (Figure 8).

Discussion

Our findings support our hypothesis that FGF-2 stimulates the tenogenic differentiation of progenitors to improve the biomechanical strength and histological appearance of repaired RCs in rats. Previous studies[6, 23] have described the healing response as observed using histological evaluation in a rat RC acute injury and immediate repair model, and the healing response occurred almost exclusively within the tendon-to-bone insertion site that was filled with hyper-cellular and hyper-vascular granulation tissues by postoperative day 10. As healing progresses, cellularity and vascularity decrease, and then the improvement of collagen fiber orientation and fiber integration into the bone were observed to some extent. However, a histologically normal tissue is not regenerated. Instead, the disorganized fibro-vascular scar interposes at the insertion site without supplementation of growth/differentiation factors.[23] Without FGF-2 administration, in this study, the fibro-vascular scar interposes between the tendon and bone even 12 weeks after RC repair surgery. In contrast, the administration of FGF-2 clearly decreased the occurrence of fibro-vascular scarring at the insertion site and increased the aligned orientation of collagen fibers at ≥4 weeks, as indicated by significantly higher histological scores (Figure 1, Table 3). Moreover, even though normal biomechanical strength was not achieved at 12 weeks postoperatively (ultimate load-to-failure, 56.7% of normal controls; stiffness, 33.3% of normal controls; ultimate load-to-stress, 35.1% of normal controls), FGF-2 administration significantly increased the biomechanical strength by 6 weeks postoperatively (Table 2). In an ovine study model on tendon-to-bone healing, the

disorganized fibro-vascular scar at the insertion site was weaker than the axially-aligned collagen fibers in the bone.[8] These results suggest that the improvement of mechanical strength by FGF-2 treatment is associated with decreases in the fibro-vascular scarring and improvement in the collagen fiber orientation at the insertion site.

Accumulating evidence suggests that *Scx*-expressing tenogenic cells can participate in a regenerative repair of tendons to promote the formation of collagen fibers with an aligned orientation, which have better tensile strength. Gulotta et al.[7] demonstrated that application of bone marrow-derived MSCs transduced with *Scx* resulted in an improvement in histological and biomechanical properties at 4 weeks postoperatively in a similar rat RC healing model. Tan et al.[22] also reported that transplantation of *Scx*-transduced tendon-derived stem cells provided better tendon repair than that of mock-transduced cells in a rat patellar tendon injury model from the histological and biomechanical viewpoints.

Our study showed that FGF-2 administration induced *Scx* expression in the cells of healing tissue 4–8 weeks postoperatively, indicating that more tenogenic progenitor cells were generated at the healing sites from the mid-to-late stages of healing (Figures 3–4). During differentiation from tenogenic progenitors to mature tenocytes, the *Scx* expression declines, while *Tnmd* is continuously expressed.[10, 18] In murine tendon development, *Scx* expression increases from E10.5 to E12.5 and decreases at E13.5, meanwhile the expression of *Tnmd* sharply increases from E13.5 and persists until the late stage in the forelimb tendon cells.[10] These temporal expression patterns of *Scx* and

Tnmd were also demonstrated in mouse patellar healing.[16] In this study, *Tnmd*-positive tenocyte-like cells were persistently observed until the later stage of healing from 4–12 weeks postoperatively. Interestingly, *Tnmd*-positive tenocyte-like cells were only observed in the area with highly oriented collagen fibers. In particular, these cells were distributed into the reparative tissues near the suturing site in the FGF-2-treated group 4–12 weeks postoperatively, which was consistent with highly oriented collagen fiber areas as shown by the histological evaluation in this study (Figure 5E). These spatial patterns of *Tnmd* expression are similar to that in the late-stage of tendon development,[18] suggesting that *Tnmd* is a useful marker for evaluating the differentiation of mature tenocyte-like cells in tendon healing.

Despite enhanced differentiation of *Tnmd*-positive tenocyte-like cells, it is unlikely that FGF-2 directly stimulated tenogenic differentiation of cells in this later phase of RC healing, since FGF-2 is known to be released from gelatin hydrogel sheets within 2 weeks.[21] Thus, the FGF-2-stimulated tenogenic repair responses in this study must be primarily mediated by the growth stimulation of undifferentiated mesenchymal cells, as indicated by a higher incidence of PCNA-positive cells at the repair sites during the early phase (Figure 2). In a mouse patellar tendon healing model,[4] undifferentiated mesenchymal progenitors migrate from a paratenon to the healing site by 1 week post-injury. Subsequently, *Scx*-expressing cells appear at ≥2 weeks, suggesting that the initial growth of undifferentiated mesenchymal progenitors have a critical role for the subsequent tenogenic differentiation of cells during the later phase of healing. In agreement with the previous *in vitro*

studies[11, 19, 25] that have shown that FGF-2 potently stimulates the self-renewal of MSCs and/or progenitor cells without a loss of potentials for the subsequent cell differentiation, we demonstrated at least in the present study that the healing process started with a better accumulation of cells expressing MSC-related markers within 2 weeks in the FGF-2-treated group (Figure 8).

There are several limitations to the current study. First, our acutely created tear and immediate repair model does not reflect chronic degenerative RC tears, and our findings in this rat model may not directly translate to humans, because the healing processes in healthy animals may not mirror the situations encountered in clinical practice. However, based on anatomical similarities between humans, this model has been widely used to investigate the mechanism of healing[6, 23, 27] and the method of healing enhancement.[7, 9, 24] Second, this study did not directly identify the function of tenogenic marker genes during the RC healing process. Further studies using a knockout model on *Scx* or *Tnmd* are required to determine the roles of these genes during the RC healing process. Third, our findings demonstrated that the biomechanical and histological values of the control group did not reach those of the FGF-2-treated group by 12 weeks. A longer time period may be necessary to understand whether the effect observed in the FGF-2-treated group will persist throughout the healing response. Fourth, the sample size, which was based on the large effect size, was relatively small, and it may be underpowered to detect significant differences. Likewise, our histological evaluation may also be underpowered, because it did not include all sections from the specimens. However, there was little or no discrepancy among our findings observed in various evaluation

methods during RC healing. Lastly, direct clinical implications for treatment may be difficult to determine from this small animal model. Currently, little is known about the biological mechanisms underlying the RC healing response.[6] Therefore, basic research on these mechanisms may provide clues in order to determine the safety, effect, dose, and method of administration in larger models. Ultimately, human clinical trials are also needed to translate these findings to clinical use.

It is not known whether FGF-2 can selectively facilitate the growth of undifferentiated tenogenic cells of a certain mesenchymal lineage. However, the enhanced expression of *Scx* and *Tnmd* genes in the mid-to-late stages indicates that a certain microenvironment favorable for the growth response of tenogenic progenitor cells to FGF-2 may be provided in the present RC healing model. Interestingly, the transient upregulation of *Sox9* detected in the FGF-2-treated group at 4 weeks postoperatively may indicate that a possible occurrence of *Sox9* and *Scx* double-positive tenogenic progenitors contributes to enthesis formation during development.[20] Thus, further analysis of the cellular components and the microenvironment at the RC repair sites will help develop clinical strategies for inducing a specific regenerative healing response in RC injuries.

References

1. Anraku Y, Mizuta H, Sei A, et al. Analyses of early events during chondrogenic repair in rat full-thickness articular cartilage defects. *J Bone Miner Metab.* 2009;27(3):272-286.
2. Chamberlain G, Fox J, Ashton B, Middleton J. Concise review: mesenchymal stem cells: their phenotype, differentiation capacity, immunological features, and potential for homing. *Stem Cells.* 2007;25(11):2739-2749.
3. Docheva D, Hunziker EB, Fassler R, Brandau O. Tenomodulin is necessary for tenocyte proliferation and tendon maturation. *Mol Cell Biol.* 2005;25(2):699-705.
4. Dyment NA, Hagiwara Y, Matthews BG, Li Y, Kalajzic I, Rowe DW. Lineage tracing of resident tendon progenitor cells during growth and natural healing. *PLoS One.* 2014;9(4):e96113.
5. Faul F, Erdfelder E, Buchner A, Lang AG. Statistical power analyses using G*Power 3.1: tests for correlation and regression analyses. *Behav Res Methods.* 2009;41(4):1149-1160.
6. Galatz LM, Sandell LJ, Rothermich SY, et al. Characteristics of the rat supraspinatus tendon during tendon-to-bone healing after acute injury. *J Orthop Res.* 2006;24(3):541-550.
7. Gulotta LV, Kovacevic D, Packer JD, Deng XH, Rodeo SA. Bone marrow-derived mesenchymal stem cells transduced with scleraxis improve rotator cuff healing in a rat model. *Am J Sports Med.* 2011;39(6):1282-1289.
8. Hee CK, Dines JS, Dines DM, et al. Augmentation of a rotator cuff suture repair using rhPDGF-BB and a type I bovine collagen matrix in an ovine model. *Am J Sports Med.* 2011;39(8):1630-1639.
9. Ide J, Kikukawa K, Hirose J, et al. The effect of a local application of fibroblast growth factor-2 on tendon-to-bone remodeling in rats with acute injury and repair of the supraspinatus tendon. *J Shoulder Elbow Surg.* 2009;18(3):391-398.
10. Liu H, Zhang C, Zhu S, et al. Mohawk promotes the tenogenesis of mesenchymal stem cells

through activation of the TGFβ signaling pathway. *Stem Cells*. 2014;33(2):443-455.

11. Lotz S, Goderie S, Tokas N, et al. Sustained levels of FGF2 maintain undifferentiated stem cell cultures with biweekly feeding. *PLoS One.* 2013;8(2):e56289.

12. Mizuta H, Kudo S, Nakamura E, Otsuka Y, Takagi K, Hiraki Y. Active proliferation of mesenchymal cells prior to the chondrogenic repair response in rabbit full-thickness defects of articular cartilage. *Osteoarthritis Cartilage.* 2004;12(7):586-596.

13. Murchison ND, Price BA, Conner DA, et al. Regulation of tendon differentiation by scleraxis distinguishes force-transmitting tendons from muscle-anchoring tendons. *Development.* 2007;134(14):2697-2708.

14. Russell RD, Knight JR, Mulligan E, Khazzam MS. Structural integrity after rotator cuff repair does not correlate with patient function and pain: a meta-analysis. *J Bone Joint Surg Am.* 2014;96(4):265-271.

15. Schweitzer R, Chyung JH, Murtaugh LC, et al. Analysis of the tendon cell fate using Scleraxis, a specific marker for tendons and ligaments. *Development.* 2001;128(19):3855-3866.

16. Scott A, Sampaio A, Abraham T, Duronio C, Underhill TM. Scleraxis expression is coordinately regulated in a murine model of patellar tendon injury. *J Orthop Res.* 2011;29(2):289-296.

17. Shukunami C, Oshima Y, Hiraki Y. Chondromodulin-I and tenomodulin: a new class of tissue-specific angiogenesis inhibitors found in hypovascular connective tissues. *Biochem Biophys Res Commun.* 2005;333(2):299-307.

18. Shukunami C, Takimoto A, Oro M, Hiraki Y. Scleraxis positively regulates the expression of tenomodulin, a differentiation marker of tenocytes. *Dev Biol.* 2006;298(1):234-247.

19. Solchaga LA, Penick K, Goldberg VM, Caplan AI, Welter JF. Fibroblast growth factor-2 enhances proliferation and delays loss of chondrogenic potential in human adult

bone-marrow-derived mesenchymal stem cells. *Tissue Eng Part A.* 2010;16(3):1009-1019.

20. Sugimoto Y, Takimoto A, Akiyama H, et al. Scx+/Sox9+ progenitors contribute to the establishment of the junction between cartilage and tendon/ligament. *Development.* 2013;140(11):2280-2288.

21. Tabata Y, Ikada Y. Vascularization effect of basic fibroblast growth factor released from gelatin hydrogels with different biodegradabilities. *Biomaterials.* 1999;20(22):2169-2175.

22. Tan C, Lui PP, Lee YW, Wong YM. Scx-transduced tendon-derived stem cells (tdscs) promoted better tendon repair compared to mock-transduced cells in a rat patellar tendon window injury model. *PLoS One.* 2014;9(5):e97453.

23. Thomopoulos S, Hattersley G, Rosen V, et al. The localized expression of extracellular matrix components in healing tendon insertion sites: an in situ hybridization study. *J Orthop Res.* 2002;20(3):454-463.

24. Thomopoulos S, Soslowsky LJ, Flanagan CL, et al. The effect of fibrin clot on healing rat supraspinatus tendon defects. *J Shoulder Elbow Surg.* 2002;11(3):239-247.

25. Tsutsumi S, Shimazu A, Miyazaki K, et al. Retention of multilineage differentiation potential of mesenchymal cells during proliferation in response to FGF. *Biochem Biophys Res Commun.* 2001;288(2):413-419.

26. Uezono K, Ide J, Tokunaga T, et al. Effect of postoperative passive motion on rotator cuff reconstruction with acellular dermal matrix grafts in a rat model. *Am J Sports Med.* 2014;42(8):1930-1938.

27. Wurgler-Hauri CC, Dourte LM, Baradet TC, Williams GR, Soslowsky LJ. Temporal expression of 8 growth factors in tendon-to-bone healing in a rat supraspinatus model. *J Shoulder Elbow Surg.* 2007;16(5 Suppl):S198-203.

28. Yokoya S, Mochizuki Y, Natsu K, Omae H, Nagata Y, Ochi M. Rotator cuff regeneration using a bioabsorbable material with bone marrow-derived mesenchymal stem cells in a rabbit

525 model. *Am J Sports Med.* 2012;40(6):1259-1268.

526

Figure legends

Figure 1: Photomicrographs of the specimens at 2, 6 and 12 weeks postoperatively (A–F: control; G–L: FGF-2-treated). The hematoxylin and eosin-stained sections (A–C, G–I) and picrosirius-red stained sections under polarized light (D–F, J–L). The boxed areas in A–C and G–I are shown at a higher magnification in a–c and g–i, respectively. Bars, 200 μm.

Figure 2: Immunostaining for the proliferating cell nuclear antigen (PCNA) at 2 and 6 weeks postoperatively (A, B: control; C, D: FGF-2-treated). The sections are counterstained with hematoxylin. Bars, 100 μm.

The percentage of PCNA-positive cells in the region of interest at the insertion site during rotator cuff healing (E). Bar graphs, the mean for each group; error bars, one standard deviation. $^{*}P < .05$, $^{**}P < .01$.

Figure 3: The gene expression levels of *Scleraxis* (A) and *Tenomodulin* (B) in the healing tissues. The target genes are normalized to *18S ribosomal RNA* expression and are further normalized to the intact supraspinatus tendon tissues that are equal to 1. Bar graphs, the mean for each group; error bars, one standard deviation. $^{*}P < .05$, $^{**}P < .01$.

Figure 4: *In situ* hybridization of *Scleraxis* and *Tenomodulin* at the tendon mid-substance (A–F,

M–R) and the insertion site (G–L, S–X) at 2 and 8 weeks postoperatively (A–L: control; M–X: FGF-2-treated). Sense, the negative control using a sense labeled probe. Arrows, the hybridization signals. Bars, 100 μm.

Figure 5: Picrosirius-red-stained sections under polarized light (A) and *in situ* hybridization of *Tenomodulin* (B) for the FGF-2-treated group at 8 weeks postoperatively. Arrows, the hybridization signals. Bars, 200 μm. Schematic illustration of the segmented area in healing tissues (C). (t, tendon areas; s, suture areas; i, insertion areas; a, articular side; m, middle layer; b, bursal side). Correlation between collagen fiber orientation and the expression levels of *Scx* mRNA (D), or *Tnmd* mRNA (E) for each area in both groups, respectively. Gray scale percentages are relative values compared to six intact specimens. The correlation coefficient (ρ) and *P*-value were obtained by Spearman's correlation analysis.

Figure 6: The gene expression levels of *Sox9* in the healing tissues. The target genes are normalized to *18S ribosomal RNA* expression and are further normalized to the intact supraspinatus tendon tissues that are equal to 1. Bar graphs, the mean for each group; error bars, one standard deviation. * $P < .05$, ** $P < .01$.

Figure 7: Immunostaining for Sox9 at 2, 4, 6, and 12 weeks postoperatively (A–D: control; E–H:

565 FGF-2-treated). The percentage of Sox9-positive cells in the region of interest at the insertion site

566 (G). The sections are counterstained with hematoxylin. Bars, 50 μm. Bar graphs, the mean for each

567 group; the error bars, one standard deviation. $^{*}P < .05$, $^{**}P < .01$.

568

569 **Figure 8:** Immunostaining for mesenchymal stem cell-related surface antigens CD105 (A, F), CD90

570 (B, G), and CD73 (C, H) and hematopoietic cell antigen CD45 (D, I) and CD34 (E, J) at the insertion

571 site at 2 weeks postoperatively. A–E (control) and F–J (FGF-2-treated) are serial sections

572 counterstained with hematoxylin. Bars, 50 μm.

573

574 Table 1

575

576

TABLE 1

The Histological Scoring System

Characteristics	Score
Cellularity (%)[a]	
> 400	1
300－400	2
200－300	3
< 200	4
Vascularity (bv/low PF)[b]	
> 15	1
10－15	2
6－10	3
< 6	4
Collagen fiber orientation (%)[c]	
< 25	1
25－50	2
50－75	3
> 75	4

[a] Number of cells per region of interest from each section; percentages represent relative values compared to the values from normal tendon-to-bone sections (n = 6), which were set at 100%.

[b] Number of blood vessels per low PF (100-fold magnification) from each section; bv, blood vessel; PF, power field.

[c] Gray scale per region of interest from each section as measured using Image J, percentages represent relative values compared to the values from normal tendon-to-bone sections (n = 6), which were set at 100%.

577 Table 2

578

579

TABLE 2

The Summary of The Biomechanical Testing[a]

Time point / group	Ultimate load-to-failure (N)	Stiffness (N/mm)	Cross-sectional area (mm^2)	Ultimate stress-to-failure (N/mm^2)
6 weeks				
Control (n = 9)	7.92 ± 2.54	3.43 ± 1.24	3.53 ± 0.51	2.34 ± 0.93
FGF-2 (n = 9)	15.1 ± 3.32 *	7.16 ± 3.28 *	3.56 ± 0.35	4.24 ± 0.96 *
P value	.009	.005	.627	.001
12 weeks				
Control (n = 9)	13.8 ± 4.69[b]	6.83 ± 1.25[b]	3.53 ±0.26	3.88 ± 1.12[b]
FGF-2 (n = 9)	23.8 ± 4.61[b] *	8.98 ± 3.58	3.42 ±0.28	6.92 ± 1.10[b] *
P value	.003	.310	.354	.003
Normal control (n = 9)	42.0 ± 5.56	27.0 ± 2.85	2.09 ± 0.13	19.7 ± 2.44

[a]All values are the mean ± standard deviation.
[b]Significantly different between time points within group ($P < .05$).
*Significantly different between groups at the same time point ($P < .01$).

580 Table 3

581

582

TABLE 3

Summary of The Histological Assessment [a]

Time point Treatment	Cellularity [b] (%)	Vascularity [c] (bv/ low PF)	Collagen fiber orientation [d] (%)	Total score [e]
2 weeks				
Control (n = 6)	552 ±72.5	35.7 ±8.4	17.9 ±2.5	3.0 ±0.0
FGF-2 (n = 6)	604 ±98.3	44.7 ±8.7	21.6 ±3.7	3.2 ±0.4
P value	.423	.109	.078	.631
4 weeks				
Control (n = 6)	448 ±56.9	31.5 ±3.4	41.4 ±10.9[f] *	4.0 ±0.6 *
FGF-2 (n = 6)	503 ±30.8	29.9 ±9.2[f]	56.0 ±3.3[f]	4.8 ±0.4
P value	.078	.689	.007	.045
6 weeks				
Control (n = 6)	447 ±49.1 *	22.7 ±5.5[f]	57.4 ±5.3[f] *	5.2 ±0.4[f,g] *
FGF-2 (n = 6)	377 ±41.2[f,g]	18.4 ±5.7[f]	68.1 ±4.8[f,g]	6.3 ±1.0[f]
P value	.025	.298	.025	.037
8 weeks				
Control (n = 6)	389 ±41.2[f]	21.6 ±6.6[f] *	62.5 ±4.6[f-h] *	5.8 ±0.4[e,f] *
FGF-2 (n = 6)	338 ±59.0[e,f]	11.4 ±4.7[f,g]	73.4 ±8.1[f,g]	8.0 ±1.7[e,f]
P value	.128	.020	.025	.013
12 weeks				
Control (n = 6)	350 ±57.2[e]	13.6 ±3.3[f,g] *	70.8 ±6.4[f-h] *	7.2 ±1.0[f-i] *
FGF-2 (n = 6)	288 ±52.5[f,g]	8.1 ±2.3[f,g]	81.9 ±4.5[f-h]	9.3 ±1.2[f-h]
P value	.109	.013	.025	.013

[a]All values are the mean ± standard deviation.

[b] Number of cells per region of interest from each section; percentages represent relative values compared to the values from normal tendon-to-bone sections (837 ± 86.3 cells/mm2, n = 6), which were set to 100%.

[c] Number of blood vessels per low PF (100-fold magnification) from each section; bv, blood vessel; PF, power field.

[d] Gray scale per region of interest from each section as measured using Image J; percentages represent relative values compared to the values from normal tendon-to-bone sections (191.0 ± 17.5 gray scale, n = 6), which were set to 100%.

[e] Scores represent a total score of three parameters including cellularity, vascularily and collagen fiber orientation. A perfect score in this scoring system is 12 points.

[f-i] Significantly different within group compared to 2(f), 4(g), 6(h), and 8 weeks(i), respectively (*P* < .05*)*.

*Significantly different between groups at the same time point (*P* < .05*)*.

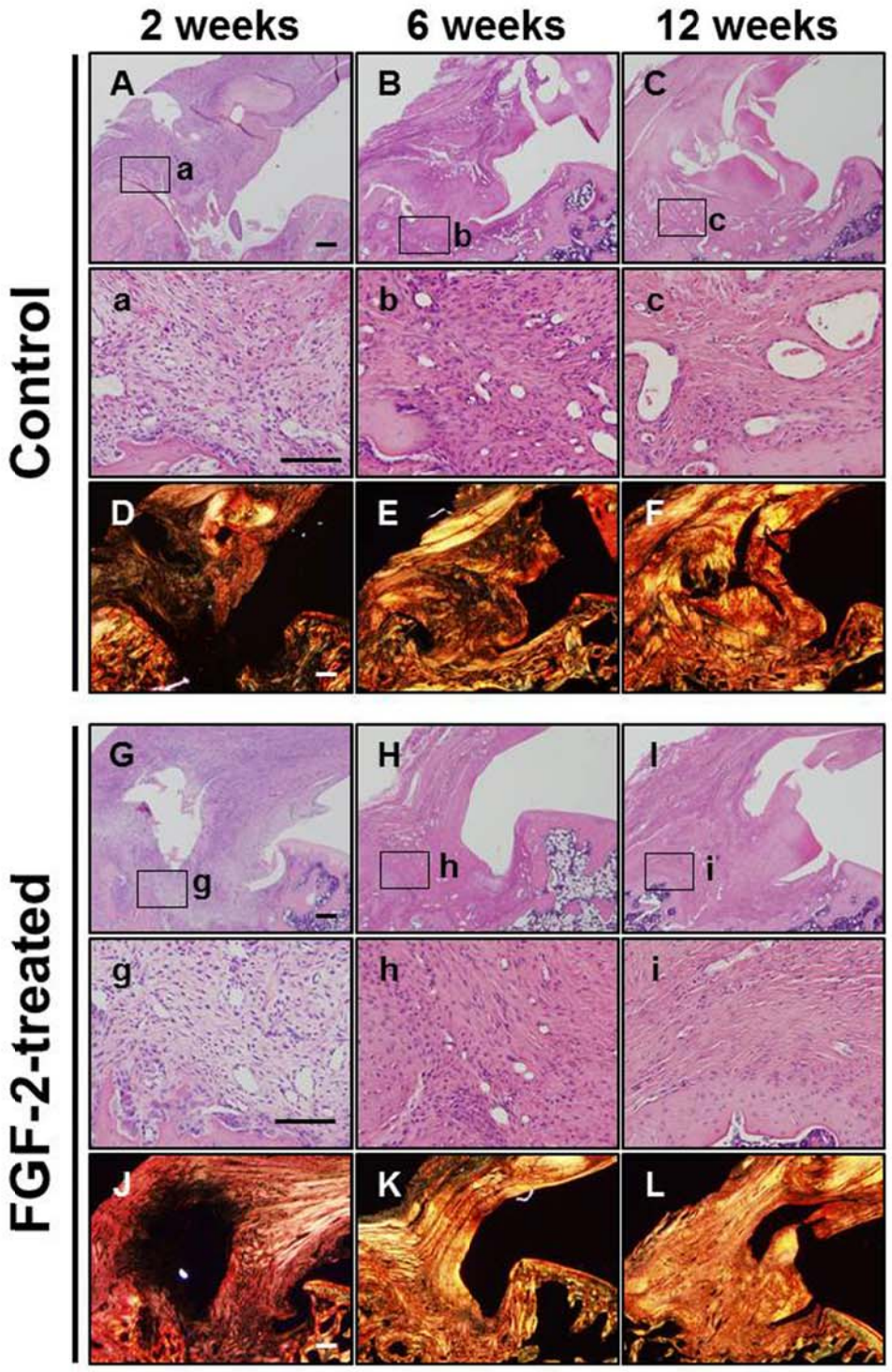

Figure 1. Photomicrographs of the specimens at 2, 6 and 12 weeks postoperatively (A–F: control; G–L: FGF-2-treated). The hematoxylin and eosin-stained sections (A–C, G–I) and picrosirius-red stained sections under polarized light (D–F, J–L). The boxed areas in A–C and G–I are shown at a higher magnification in a–c and g–i, respectively. Bars, 200 μm.

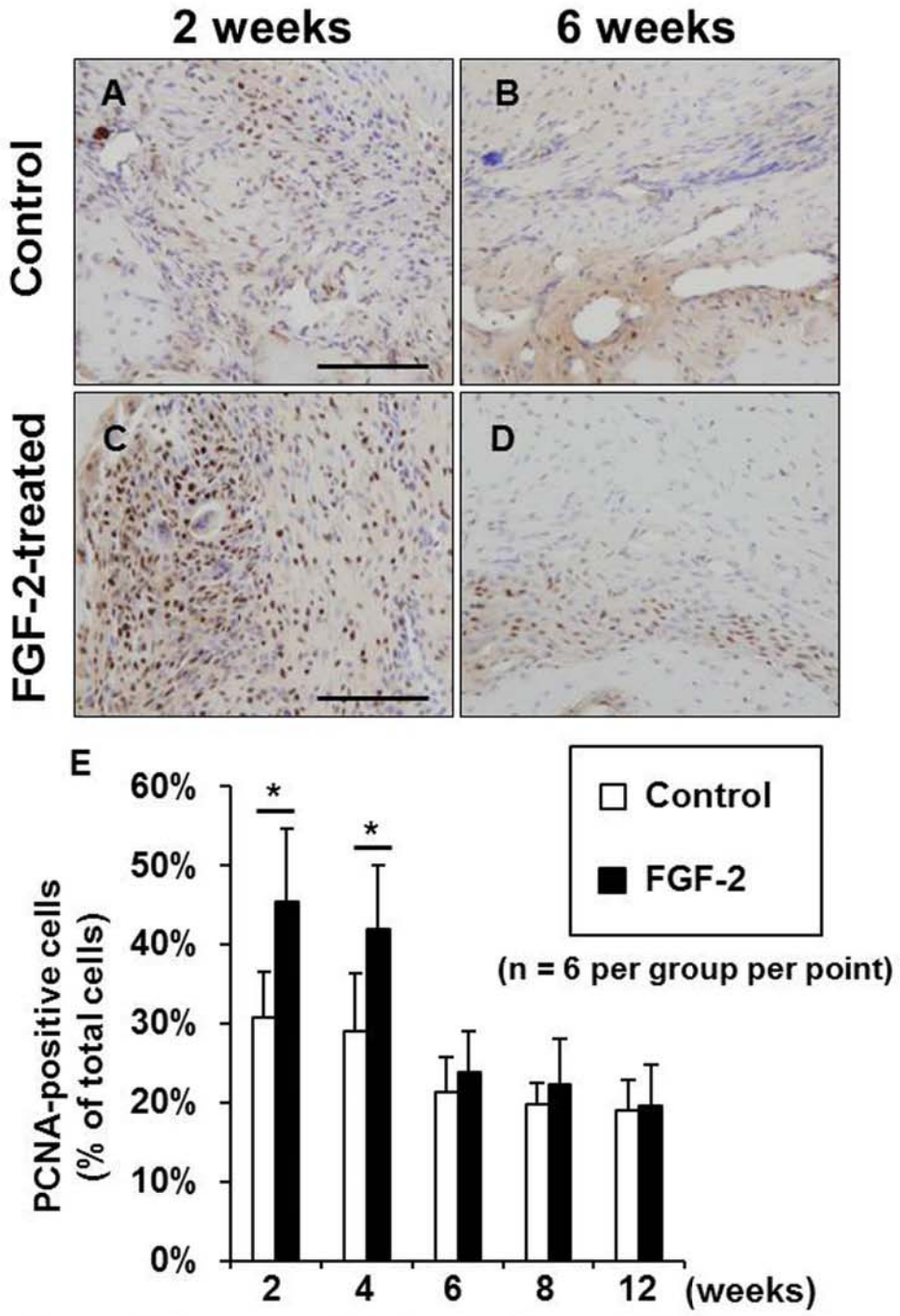

Figure 2. Immunostaining for the proliferating cell nuclear antigen (PCNA) at 2 and 6 weeks postoperatively (A, B: control; C, D: FGF-2-treated). The sections are counterstained with hematoxylin. Bars, 100 μm.

The percentage of PCNA-positive cells in the region of interest at the insertion site during rotator cuff healing (E). Bar graphs, the mean for each group; error bars, one standard deviation. $^{*}P < .05$, $^{**}P < .01$.

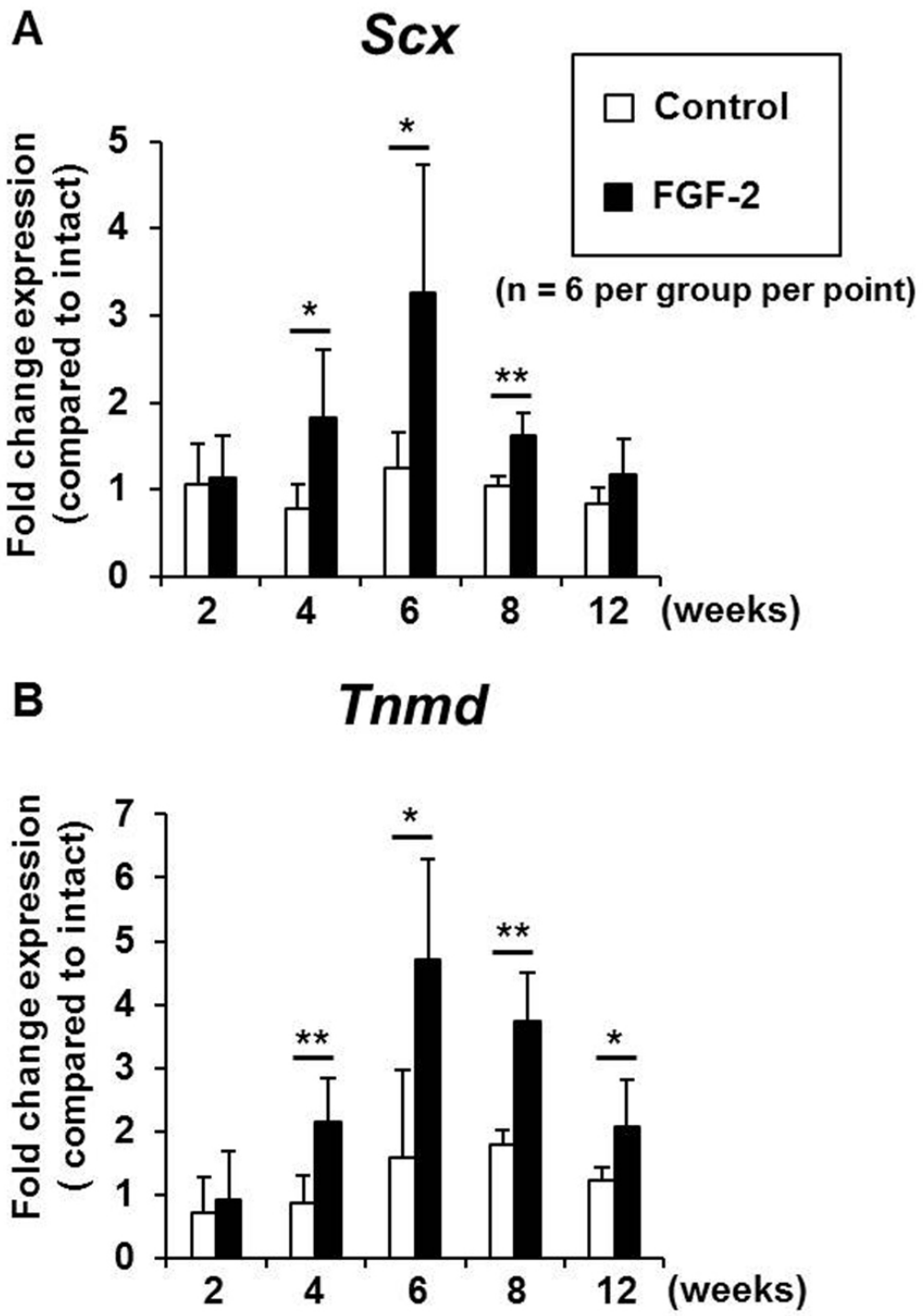

Figure 3. The gene expression levels of *Scleraxis* (A) and *Tenomodulin* (B) in the healing tissues. The target genes are normalized to *18S ribosomal RNA* expression and are further normalized to the intact supraspinatus tendon tissues that are equal to 1. Bar graphs, the mean for each group; error bars, one standard deviation. $^{*}P < .05$, $^{**}P < .01$.

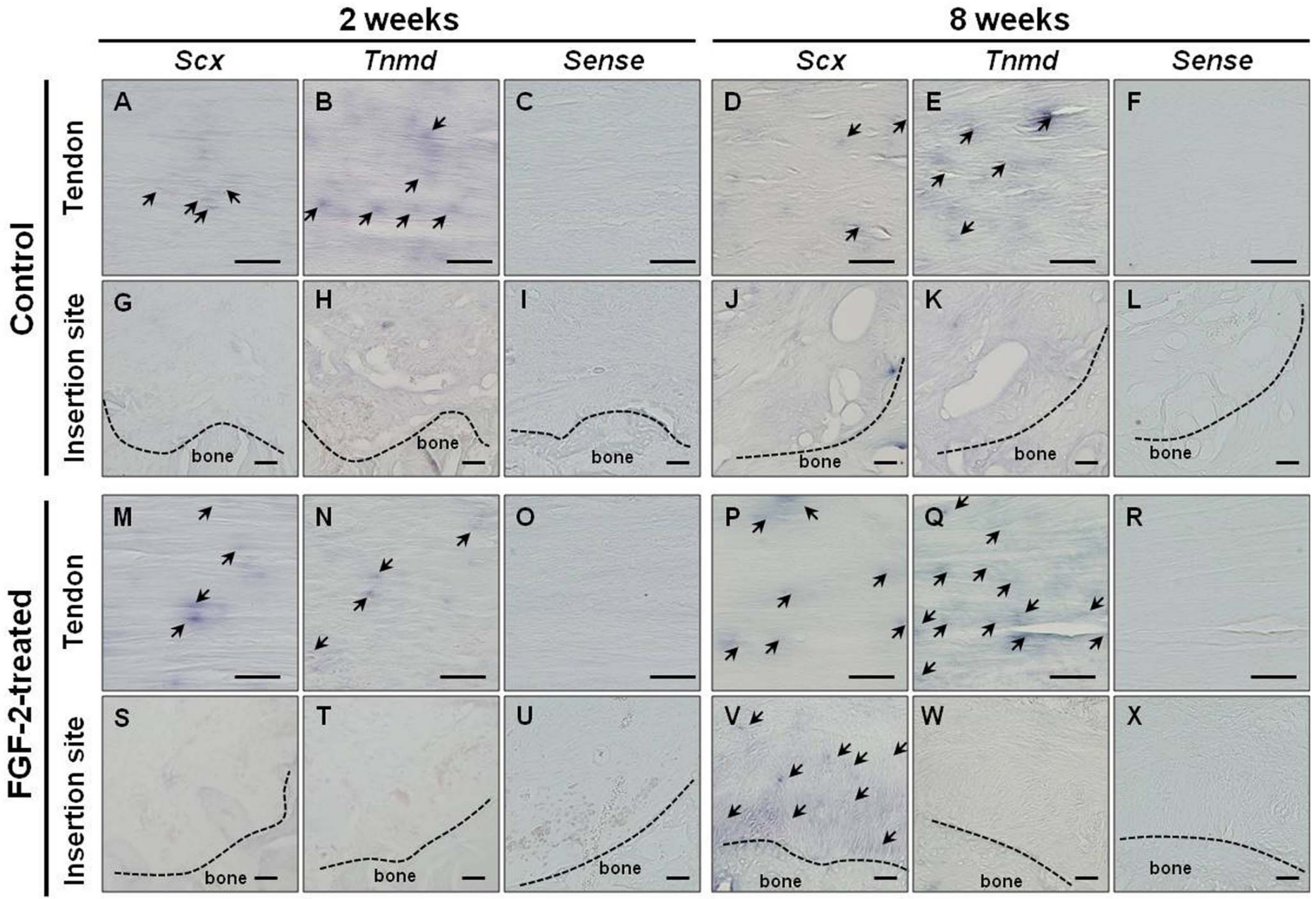

Figure 4. *In situ* hybridization of *Scleraxis* and *Tenomodulin* at the tendon mid-substance (A–F, M–R) and the insertion site (G–L, S–X) at 2 and 8 weeks postoperatively (A–L: control; M–X: FGF-2-treated). Sense, the negative control using a sense labeled probe. Arrows, the hybridization signals. Bars, 100 μm.

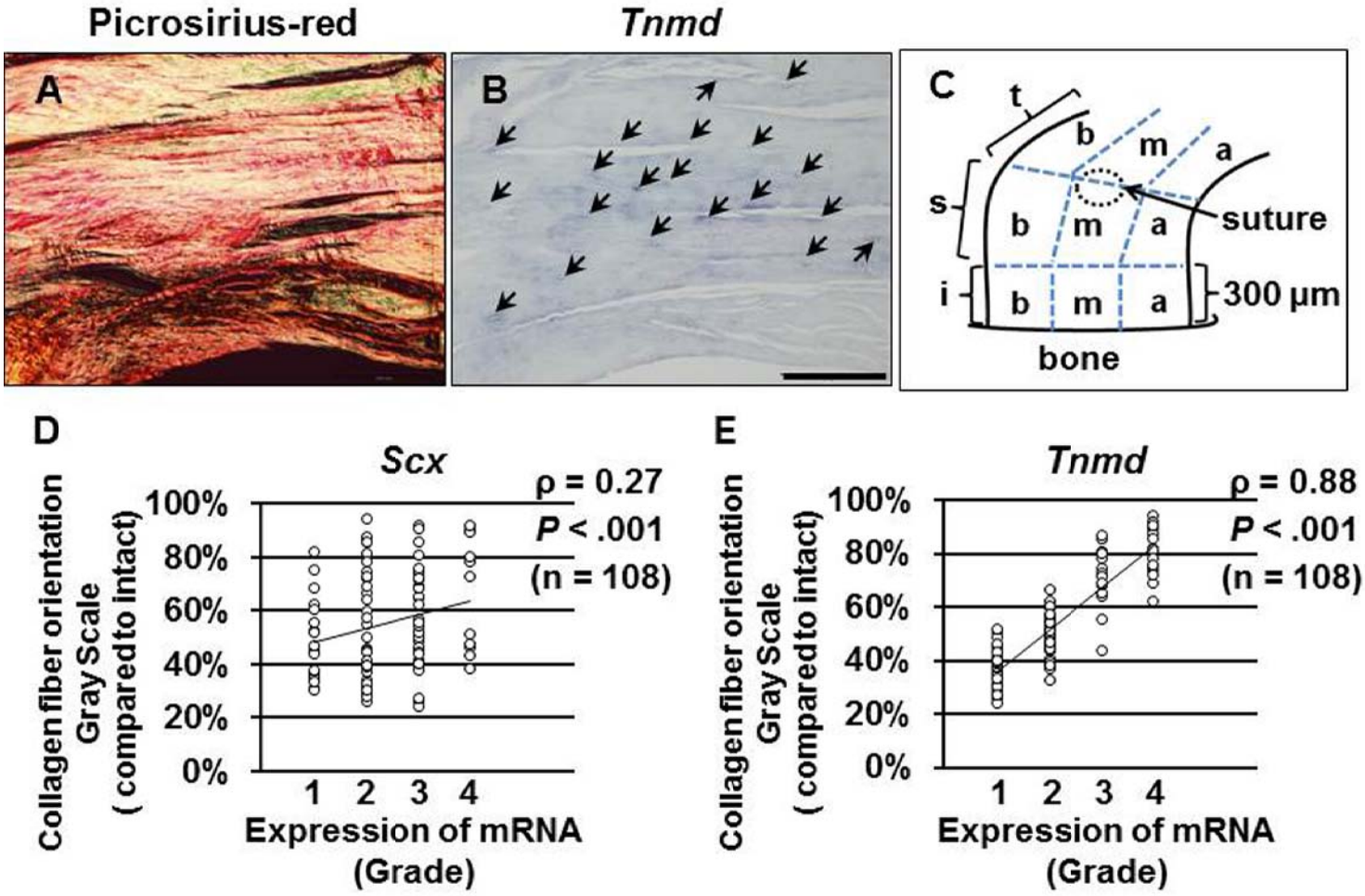

Figure 5. Picrosirius-red-stained sections under polarized light (A) and *in situ* hybridization of *Tenomodulin* (B) for the FGF-2-treated group at 8 weeks postoperatively. Arrows, the hybridization signals. Bars, 200 μm. Schematic illustration of the segmented area in healing tissues (C). (t, tendon areas; s, suture areas; i, insertion areas; a, articular side; m, middle layer; b, bursal side). Correlation between collagen fiber orientation and the expression levels of *Scx* mRNA (D), or *Tnmd* mRNA (E) for each area in both groups, respectively. Gray scale percentages are relative values compared to six intact specimens. The correlation coefficient (ρ) and *P*-value were obtained by Spearman's correlation analysis.

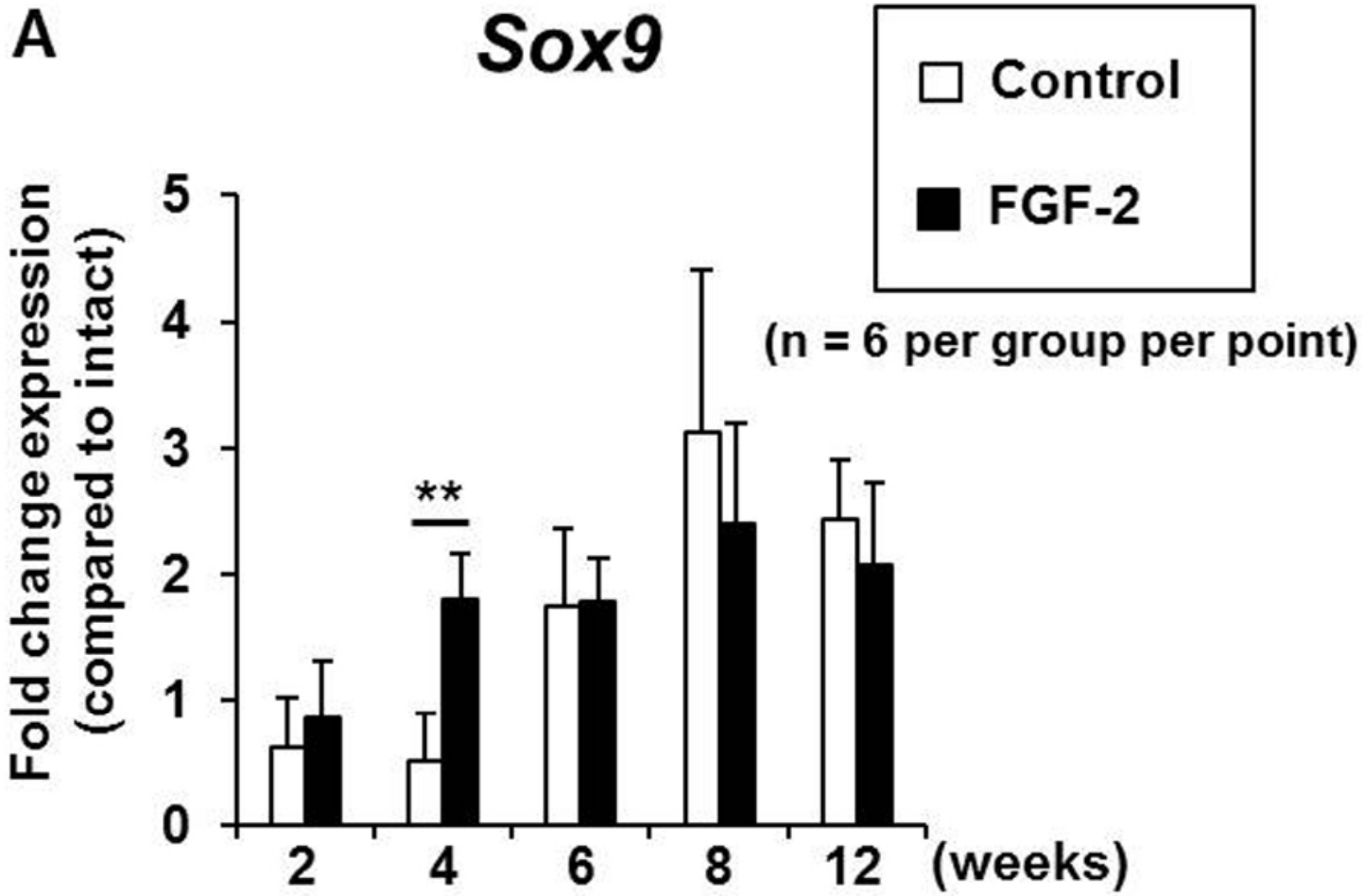

Figure 6. The gene expression levels of *Sox9* in the healing tissues. The target genes are normalized to *18S ribosomal RNA* expression and are further normalized to the intact supraspinatus tendon tissues that are equal to 1. Bar graphs, the mean for each group; error bars, one standard deviation. $^{*}P < .05$, $^{**}P < .01$.

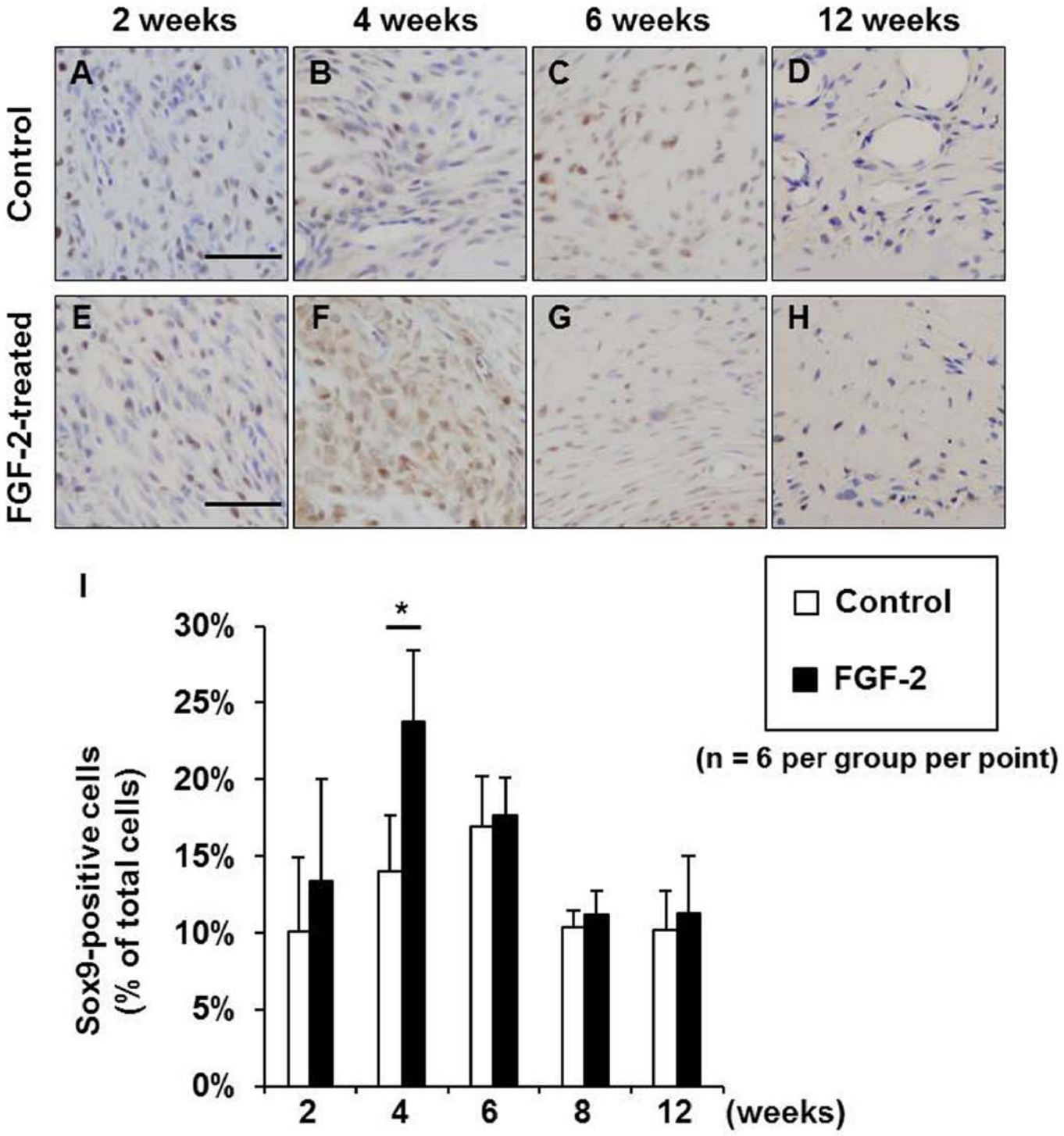

Figure 7. Immunostaining for Sox9 at 2, 4, 6, and 12 weeks postoperatively (A–D: control; E–H: FGF-2-treated). The percentage of Sox9-positive cells in the region of interest at the insertion site (G). The sections are counterstained with hematoxylin. Bars, 50 μm. Bar graphs, the mean for each group; the error bars, one standard deviation. $^{*}P < .05$, $^{**}P < .01$.

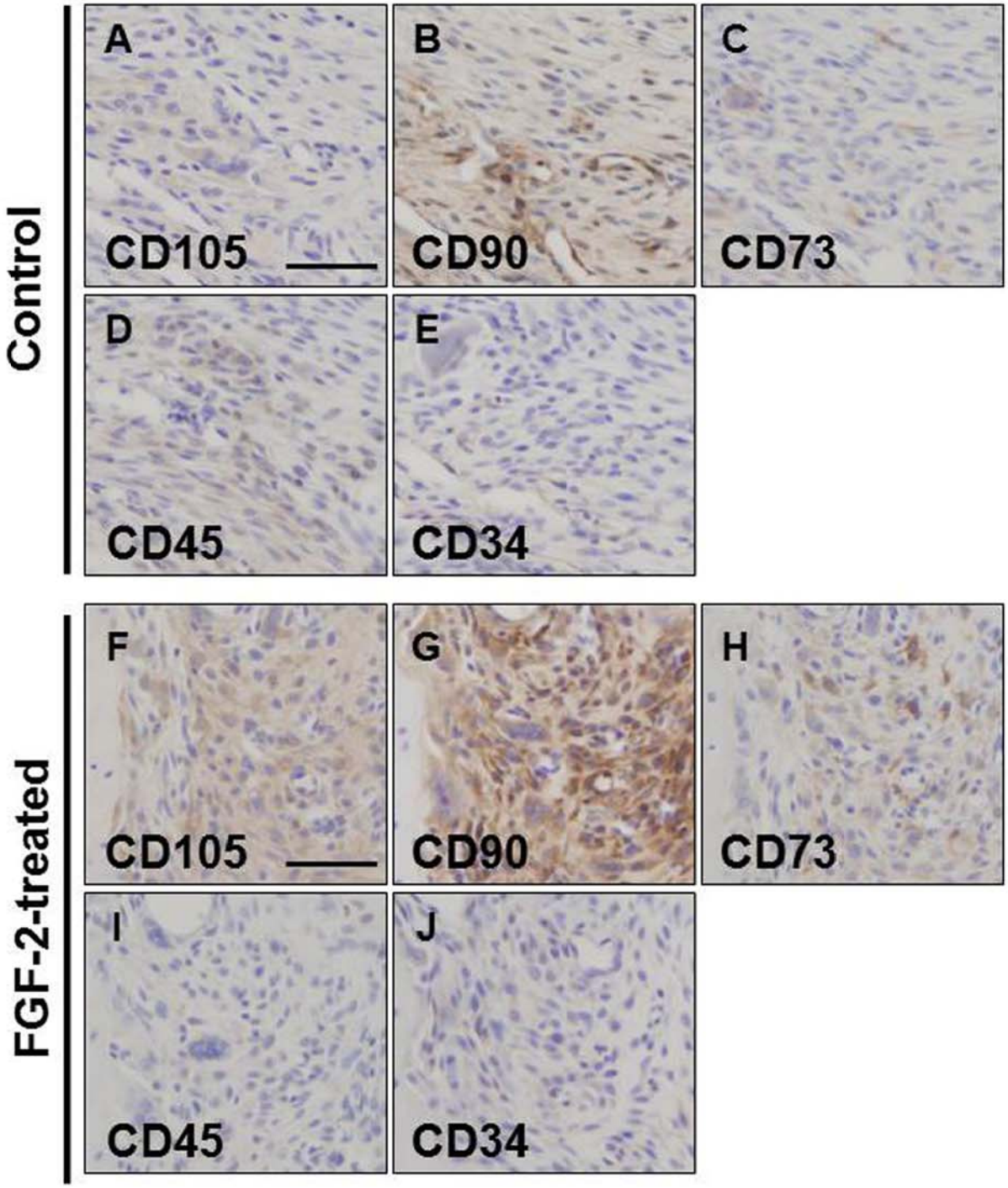

Figure 8. Immunostaining for mesenchymal stem cell-related surface antigens CD105 (A, F), CD90 (B, G), and CD73 (C, H) and hematopoietic cell antigen CD45 (D, I) and CD34 (E, J) at the insertion site at 2 weeks postoperatively. A–E (control) and F–J (FGF-2-treated) are serial sections counterstained with hematoxylin. Bars, 50 μm.